Simultaneous removal of heavy metals and dyes in water using a MgO-coated Fe_3O_4 nanocomposite: Role of micro-mixing effect induced by bubble generation

Manoj P. Rayaroth [a, b], Dasom Oh [a], Chung-Seop Lee [a], Yoon-Seok Chang [a*]

[a] Division of Environmental Science and Engineering, Pohang University of Science and Technology (POSTECH), Nam-gu, Pohang, 37673, Republic of Korea.

[b] Department of Process Engineering and Chemical Technology, Faculty of Chemistry, Gdansk University of Technology, 80-233 Gdańsk, 11/12 Narutowicza Str, Poland

*** Corresponding author**

Prof. Dr. Yoon-Seok Chang

Division of Environmental Science and Engineering

Pohang University of Science and Technology (POSTECH)

Pohang 37673, Republic of Korea

Tel.: +82 54 279 2281; Fax: +82 54 279 8299

Email address: chang.yoonseok@postech.ac.kr

Abstract:

This study focused on the development of a nano-adsorbent for contaminant removal without the use of any external energy. An eco-friendly Fe_3O_4@MgO core-shell nanocomposite was synthesized and tested for the removal of a heavy metal, lead (Pb^{2+}) and a dye, rhodamine B (RhB). The addition of H_2O_2 into the system enabled the self-mixing of the aqueous solution containing Fe_3O_4@MgO through the generation of bubbles. This system showed an excellent removal efficiency of 99% in just 15 min for Pb^{2+} and 120 min for RhB, which is far better than the control experiment (without H_2O_2). The cation exchange mechanism dominated in the removal of heavy metals, while the adsorptive removal of dye proceeded through the H-bonding between $Mg(OH)_2$ and dye molecules. The removal efficiency increased exponentially with the increase of H_2O_2 at the optimal concentration of 5% and it was effective over a wide pH range. Moreover, the performance of the Fe_3O_4@MgO-H_2O_2 system was verified for other heavy metals such as Cd, Ni, Zn, Co, and Cu, demonstrating that the Fe_3O_4@MgO-H_2O_2 system can be widely implemented in the treatment of real water matrices contaminated with heavy metals and organic dyes.

Keywords: *Water treatment, Fe_3O_4@MgO, bubble generation, adsorption, heavy metals, dyes*

Abbreviations

RhB: rhodamine B, PEG: Polyethylene glycol, CTAB: Cetyltrimethylammonium bromide, SEM: scanning electron microscopy, EDX: Energy dispersive X-ray, XRD: X-ray diffractometer, XPS: X-ray photoelectron spectroscopy, ICP-OES: inductively coupled plasma–optical emission spectrometer, DO: Dissolved oxygen

1. Introduction

Heavy metals such as arsenic, lead, cadmium, nickel, chromium, cobalt, and selenium are major environmental pollutants because of their toxic effects, even at trace levels (Nadeem et al., 2006; Qiu et al., 2021). All these elements are discharged directly from industries and agricultural fields into the aquatic system. Their adverse effects create negative impacts on all environmental compartments (Vakili et al., 2014). Although there are several sources of the exposure of humans to these pollutants, their intake via drinking water is the most prominent and thereby highlights the need for a proper treatment protocol. Another important category of water pollutants is dye waste (Nigam et al., 1996) which is introduced into water bodies from textile mills, leather, jute, and food industries. Previous reports showed that dyehouse effluent contains many heavy metals, which also increase the perilous situation of water pollution by this kind of waste (Chen et al., 2007; Ye et al., 2021b). However, traditional technologies such as ion exchange, biological degradation, reverse osmosis, coagulation and flocculation, membrane filtration, oxidation, and chemical precipitation are effective mostly in the removal of a single pollutant from various contaminated water (Dotto et al., 2019; Rasaki et al., 2019; Zazou et al., 2019; Iqbal et al., 2021). Therefore, recent studies have focused on the materials/methods that could remove both heavy metals and organic pollutants in water (Kim et al., 2018; Ghaedi et al., 2022; Malik et al., 2022).

Adsorption using various nanomaterials is the most frequently used technique for the removal of a majority of pollutants (Valix et al., 2004; Afroze and Sen, 2018; Abdullah et al., 2019; Joseph et al., 2019; Castro-Muñoz et al., 2021; Osagie et al., 2021). However, it was found not to be very effective, especially when dealing with a mixture of pollutants. Therefore, the selection of an adsorbent that is capable of removing both organic and inorganic pollutants is a typical challenge in this field. Another difficulty is the requirement of additional mechanical

forces to increase the mass transfer of the pollutant to enhance removal efficiency, which limits the practical implementation of adsorption materials. Recent advances in environmental nanotechnology have therefore focused on decontamination using self-propelled materials (Calvo-Marzal et al., 2010; Liu et al., 2010; Sánchez et al., 2015; Wang and Pumera, 2015; Chen et al., 2017; Xu et al., 2017). Pt/Fe-, MnO_2-, and Ag-based materials have been widely deployed as self-propelled materials in the presence of certain chemicals for water purification (Ye et al., 2017; Chen et al., 2018; Lee et al., 2018; Ye et al., 2018). These materials decompose hydrogen peroxide fuel (H_2O_2) and generate bubbles to move the adsorbent through the aqueous environment. The bubble generating materials are therefore of considerable interest because of their enhanced micro-mixing capability owing to bubble propulsion, which increases pollutant transfer from the solution phase to the surface of the adsorbent and thereby improves the removal of pollutants through oxidation/adsorption processes (Gao et al., 2013b; Safdar et al., 2015; Vilela et al., 2016; Lee et al., 2018). However, the major difficulty in handling these adsorbents is the requirement for expensive supporting metals such as Pt, Au, and Ag, which can cause toxic effects when released into the aquatic system. Hence, current research is focused on environmentally friendly, stable, and easily accessible materials for such applications (Chen et al., 2018).

Metal oxide nanocomposites containing Fe_3O_4 have attracted considerable interest for environmental remediation owing to their excellent magnetic and surface properties (Kim et al., 2013; Kang et al., 2019). MnO_2-coated iron oxides have been demonstrated as an effective material for the removal of water pollutants. Kim et al. reported that these composite materials are effective for the removal of heavy metals, but require mechanical stirring (Kim et al., 2013). Moreover, Kang et al. utilized the same material in advanced oxidation processes and adsorptive

bubble separation of various dyes in the presence of a surfactant and H_2O_2 (Kang et al., 2019). These materials have also been found effective for the simultaneous removal of organics and microplastics by the micro-mixing effect (Ye et al., 2021a). However, both studies used surfactants for the generation of bubbles and the subsequent micro-mixing effect (Kang et al., 2019; Ye et al., 2021a). Surfactants are also considered an important water pollution source all over the world (Sasi et al., 2021). Therefore, for practical uses, the present study attempted to utilize nanomaterials that are capable of removing both organic and inorganic contaminants from aqueous bodies without the use of surfactants or other fuels.

Mg, one of the most abundant elements in the world, is characterized by its high reactivity in water and air to form oxides and hydroxides. These reactions evolve H_2 gas to enable the propulsion of particles in water. Therefore, many studies have evaluated materials such as TiO_2, Au/TiO_2, Au, and Ag-doped with Mg, which are used for the removal of a variety of organic pollutants (Gao et al., 2013a; Mou et al., 2013; Li et al., 2014; Vilela et al., 2017). Instead, the lifetime of the H_2 generation reaction is relatively short because of the rapid corrosion reaction (Mou et al., 2013). The formation of a passivation layer of the corresponding hydroxide hinders the further reduction of water. Mg-based alkaline materials like MgO are considered an efficient material for the remediation of pollutants through adsorption owing to their high adsorption capacity (Gao et al., 2008; Yu et al., 2011; Kameda et al., 2018; Chinthala et al., 2021). The MgO nanoparticles are not expensive and environmentally benign, and can hence be easily used to scale up the removal process. Moreover, *in vivo* toxicity evaluations, it has shown that these particles are relatively less toxic than other metal oxides (TiO_2, MnO_2, ZnO, etc.,) and also biocompatible (Gao et al., 2008; Sasaki et al., 2011; Yu et al., 2011). Therefore, MgO in conjunction with other materials (graphene, graphene oxide and diatomite, Fe–Co–Mn

nanoparticles) has been widely utilized for the removal of heavy metals and many organic pollutants (Mohan et al., 2017; Rahdar et al., 2019; Liu et al., 2020; Guo and Bulin, 2021). A disadvantage of this process is the required mechanical stirring and separation of the material after the adsorption process. Thus, the key objective of the present study was the development of a MgO-based and easily separable/recoverable material for the removal of pollutants without external agitation.

Similar to MnO_2, MgO decomposes H_2O_2 to generate O_2 gas (Zeng et al., 2020), which is assumed to be helpful in the bubble-induced mixing of the particles. Thus, the combination of MgO with Fe_3O_4 nanoparticles (Fe_3O_4@MgO) was proposed as an efficient material for water treatment. All the previously reported micro-mixing and bubble generating systems used surfactants to induce bubble formation. In addition, they had focused on only one kind of pollutants (either organic or inorganic) in their removal. In contrast to the previous reports, this study tried to remove both kinds of pollutants simultaneously without the use of surfactants. In short, the objectives of the present study were i) to investigate the mechanism of bubble generation and the micro-mixing capacity, ii) to study the potential of Fe_3O_4@MgO nanocomposite for concomitant removal of Pb^{2+} and rhodamine B dye without any mechanical stirring, and iii) to evaluate the applicability of the Fe_3O_4@MgO micro-mixing system to real contaminated water spiked with the selected model compounds.

2. Experimental section

2.1. Materials and methods

Ferric chloride ($FeCl_3$), magnesium chloride ($MgCl_2$), sodium acetate, ammonium hydroxide (NH_4OH), rhodamine B (RhB), and H_2O_2 were acquired from Merck (Seoul, South

Korea). Lead nitrate ($PbNO_3$), polyethylene glycol (PEG), and cetyltrimethylammonium bromide (CTAB) were purchased from Sigma-Aldrich (Seoul, South Korea). Ultrapure water with a specific resistivity of >18 MΩ cm was prepared using a Millipore (France) system.

2.2. Synthesis of Fe_3O_4@MgO

Fe_3O_4@MgO was synthesized using a two-step process as reported earlier (Peng et al., 2016). First, Fe_3O_4 nanoparticles were synthesized. In this step, 5 mM of $FeCl_3$ was prepared in ethylene glycol. Sodium acetate (3.6 g) and PEG (1.0 g) were added to the previously prepared $FeCl_3$ solution and stirred well at 50 °C for approximately 30 min. The mixture was then added to a 100 mL Teflon-lined autoclave and heated to 200 °C for approximately 8 h. The obtained black product of Fe_3O_4 was allowed to reach 22-25 °C room temperature and was then centrifuged, washed several times with ethanol, and dried in a vacuum oven at 60 °C for 6 h (Deng et al., 2005). Approximately 0.5 g of the previously prepared Fe_3O_4 was dispersed in 100 mL of 0.025 M CTAB and sonicated for 30 min. The solution was then mixed with 50 mL of 0.5 M $MgCl_2$ solution by constant stirring for another 1 h. NH_4OH was then added slowly to the solution to reach a temperature of 70 °C. The solution was allowed to cool until room temperature was reached. The separated particles were then washed several times with ethanol and dried at 50 °C for 6 h. The Fe_3O_4@MgO nanocomposites were then obtained by the calcination of the dried particles at 450 °C for 3 h (Peng et al., 2016).

2.3. Characterization of MgO@Fe_3O_4

The morphology and structure of the MgO@Fe_3O_4 nanocomposites were determined through scanning electron microscopy (SEM) (JSM-7401F; JEOL, Tokyo, Japan). Energy dispersive X-ray (EDX) mapping was performed to obtain the surface composition of the materials. The

crystalline nature of the material was obtained using an X-ray diffractometer (XRD, MXP18 HF; MAC Science Co., Japan). The chemical composition of the particles was analyzed using X-ray photoelectron spectroscopy (XPS, K-Alpha; Thermo Scientific, USA). The bubble formation was monitored, and images were captured using an optical microscope (Olympus MX51).

2.4. Batch experiment and analysis

Initially, a stock solution of RhB and Pb^{2+} with a concentration of 500 mg L^{-1} was prepared in deionized water. The pollutant solutions for the adsorption experiment were prepared from this stock solution. To study the removal efficiency in a real system, Pb^{2+} ions were spiked in real groundwater (from a rural area in South Korea) and river water (collected from Hyeongsan River, South Korea). Adsorption studies were conducted in a 20 mL glass vial. The solutions (10 mL) containing 10 mg L^{-1} pollutants (Pb^{2+} and RhB), and H_2O_2 were first prepared in the vial. A specific amount of Fe_3O_4@MgO was weighed and transferred into the vial. After a predetermined time interval, the materials were separated using a magnet, and approximately 200 µL of the solution was pipetted out for the analysis of the remaining pollutant in the solution. The reusability of the Fe_3O_4@MgO nanocomposite was evaluated with the addition of 10 mg L^{-1} of the selected pollutants to the magnetically separated material after 15 min of each cycle.

The concentration of Pb, Mg, and Fe ions after each sampling was analyzed using an inductively coupled plasma–optical emission spectrometer (ICP-OES, iCAP6300; Thermo Scientific). The concentration of RhB was monitored using a UV spectrophotometer at a wavelength of 540 nm (Varian, Palo Alto, CA, USA). An Orion™ Versa Star advanced electrochemistry meter was used to monitor the changes in pH and dissolved oxygen (DO) concentrations during the reaction. The removal percentage was then calculated using the eqn. 1,

$$\%\, removal = \frac{(C_o - C_t)\times 100}{C_0} \qquad (1)$$

C_0 and C_t are the concentrations of the pollutants before and after the adsorption reactions in mg/L.

3. Results and Discussions

3.1. Characterization of Fe_3O_4@MgO

As can be seen from Figs. 1A and 1B, the Fe_3O_4@MgO nanocomposite was spherical in shape. The EDX mapping showed that compared to Fe, Mg was the major contributor to the surface of the material (Fig. 1C).

Fig. 1.

The diffraction peaks at 30.2°, 35.6°, 42.9°, 53.7°, 57.2°, and 62.3° could be indexed to the cubic structure of Fe_3O_4; whereas those at 18.2°, 36.8°, 38.1°, 42.9°, and 62.3° represented the polycrystalline cubic structure of MgO. Moreover, the lack of extra peaks or peak shifts observed in the XRD spectrum confirmed that no direct interaction occurred between the core Fe_3O_4 and the outer MgO layer (Peng et al., 2016). The XPS spectrum also showed the presence of Fe, Mg, and O in the material (Fig. S1). The high-resolution Mg 1s and O 1s spectra of Fe_3O_4@MgO are shown in Fig. 2. The deconvolution of Fe 2p spectra generated four major peaks which correspond to Fe^{2+} (723.8 and 710.6 eV) and Fe^{3+} (725.3 and 711.9 eV) (Fig. S2) (Grosvenor et al., 2004). Mg 1s spectra showed peaks at 1301.7 and 1304.7 for $Mg(OH)_2$ and MgO, respectively. This was further confirmed from the corresponding O 1s peaks at 530.1and 531.2 eV corresponding to the Mg oxide (Khairallah et al., 2012; Alla et al., 2016).

Fig. 2.

3.2. Bubble generation and mixing phenomena

The prime objective of the study was to identify the micro-mixing phenomena by the generation of bubbles. The bubble generation was monitored without and with the addition of H_2O_2. The 1 mL of the aqueous solution containing different concentration of H_2O_2 (0%, 0.05%, 0.5%, 1%, 2%, 5%, and 10%) was put in a petri dish and 1 mg of Fe_3O_4@MgO added. The bubbles are then monitored using the optical microscope. The Fe_3O_4@MgO nanocomposites were aggregated and settled at the bottom once it was added to the aqueous solution. However, self-movement of the particles was observed with the generation of bubbles in the solution when H_2O_2 was added to the solution (Supporting Information Video S1). A small amount of surfactant (0.05%) was used to help monitor the bubble formation when using an optical microscope. The visual images of bubble formation in the solution containing Fe_3O_4@MgO with the addition of H_2O_2 are shown in Figs. 3A–C. Initially, the bubbles were generated around the material, then spread through the solution after 60 s, and finally, the entire solution was covered by the bubbles. This process continued for more than 2 min (Video S1). The bubble formation with the addition of different concentrations of H_2O_2 was monitored using an optical microscope and the results are shown in Figs. 3D–I. It can be seen from Fig. 3D that the bubbles were generated even in the presence of a low H_2O_2 concentration of 0.05% and the bubble formation and mixing of the nanocomposite in the solution increased with the increase in H_2O_2 addition. An interesting

observation was that the frequency of bubble generation in the medium increased until an H_2O_2 concentration of 5%.

Fig. 3.

The mechanism for bubble generation in Fe_3O_4@MgO in the presence of H_2O_2 can be explained as follows. The reaction of H_2O_2 with MgO results in the formation of MgO_2 (Eq. 2) (Zeng et al., 2020). Peroxides are well known for their oxygen generation ability when they are hydrolyzed in an aqueous medium (Eq. 3). Therefore, we could not spot distinguishable peaks for O 1s spectra for the corresponding peroxides (532.4 eV for Mg-O_2) (Deng et al., 2005). At the same time, the high-resolution Mg 1s spectra show an increase in the peak intensity at 1301.3 eV for $Mg(OH)_2$ after the reaction with H_2O_2. In addition, a small shift in the binding energy was also observed after oxidation. Further pieces of evidence for the generation of O_2 and $Mg(OH)_2$ were obtained by monitoring the pH and DO (Figs. 4A and B). The initial increase in DO of the solution in the medium is likely owing to the oxygen formation reaction. After the reaction was completed, the oxygen in the medium was removed and the DO decreased. Similarly, the pH of the medium increased from the initial 4.2 to 9.0 (Fig. 4). This is an indication of $Mg(OH)_2$ formation and its release into the water.

$$MgO + H_2O_2 \rightarrow MgO_2 + H_2O \quad (2)$$

$$MgO_2 + H_2O \rightarrow Mg(OH)_2 + O_2 \quad (3)$$

Fig. 4.

3.3. Applicability of the Fe_3O_4@MgO-H_2O_2 system for the removal of contaminants

The second objective of the study was the evaluation of the micro-mixing system in the removal of water pollutants. To evaluate the applicability of the material for environmental remediation purposes, both organic and inorganic contaminants were selected. The inorganic contaminant described in this section was Pb^{2+} and the organic contaminant selected was a dye, RhB. Fe_3O_4@MgO was added to the aqueous solution containing 10 mg L^{-1} of pollutants (Pb^{2+} and RhB), with H_2O_2 (5 %). The removal efficiencies of Pb and RhB in the mixed environment are shown in Fig. 5. As shown by the results of this study, nearly 100% of the initial Pb^{2+} and RhB were removed from the solution after 2 h. In particular, the removal of Pb^{2+} was rapid in the initial stage of the process and slowed down after 30 min, likely owing to the competition for the adsorption sites with RhB.

Fig. 5.

To better understand the mechanism of heavy metal removal, further investigation was performed with Pb^{2+}. Using ICP-OES, a constant release of Mg^{2+} to the solution was observed during the process of Pb removal (Fig. 6A). This indicates that the major mechanism for the removal of heavy metals would be the cation exchange process (Cao et al., 2012); the Mg^{2+} ions on the surface of the material are replaced with the positively charged heavy metal ions. As described in the previous section, the surface of the material is covered with $Mg(OH)_2$ and can react with the heavy metal ions to form $Pb(OH)_2$ with the release of Mg^{2+} to the solution (Eq. 4). The formation of $Pb(OH)_2$ on the surface of the material after Pb adsorption was confirmed by XPS analysis (Fig. 6B). The Pb 4f peaks located at 137.5 and 142.3 eV represent the lead oxides formed by the cation exchange process (Lai et al., 2019).

$$Mg(OH)_2 + Pb^{2+} \rightarrow Pb(OH)^2 + Mg^{2+} \quad (4)$$

Fig. 6.

The organic dye removal process follows two possible mechanisms, either through the Fenton oxidation by released Fe^{2+} or by the adsorption on the surface of the nanocomposite. As Fe_3O_4 is present in the core, its direct reaction with H_2O_2 (Fenton reaction) to generate reactive oxygen species is unlikely. To confirm this, the Fe concentration leached into the solution was monitored and a very small concentration of 0.6 mg L^{-1} of Fe was detected (Fig. S3). The homogeneous Fenton reactions with this particular Fe and Mg concentration show that the removal of RhB was insignificant (Fig. S4). Therefore, the removal of RhB is mainly through physical adsorption. As described in Eqs. 2 and 3, the first step is the formation of $Mg(OH)_2$. As reported for similar adsorbents, the hydrogen bonding between –OH present in the $Mg(OH)_2$ and nitrogen in the dye molecule favors the adsorptive removal of these types of dyes (Scheme 1) (Lin and Wang, 2009).

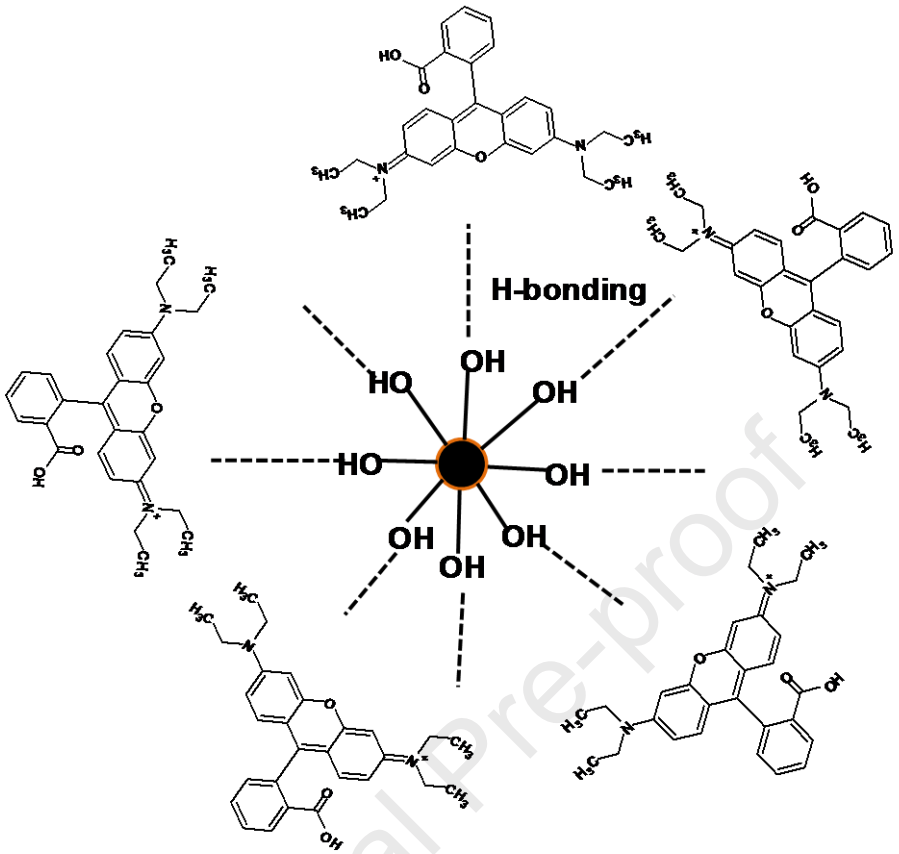

Scheme 1: Mechanism for the adsorptive removal of RhB in the Fe_3O_4@MgO-H_2O_2 system

3.4. Effects of operational parameters

The removal efficiency of the process depends on various factors such as concentrations of Fe_3O_4@MgO, H_2O_2, and the initial pH. Hence, to obtain a better performance of the system, the removal efficiency was evaluated at varying concentrations of the nanomaterial and H_2O_2 and pH. The results of Pb^{2+} removal under varying operating conditions are presented in Fig. 7 and that of RhB are shown in Supporting Information (Fig. S5).

Effect of H_2O_2 concentration

The H_2O_2 concentration (0–10%) influenced the adsorption of Pb^{2+} (10 ppm) at a fixed Fe_3O_4@MgO dose (0.8 g L^{-1}) (Fig. 7A). The removal efficiency of 20% was observed without the addition of H_2O_2, and the removal efficiency increased with the increase of reaction time. Interestingly, it is clear from Fig. 3H that even a small addition of H_2O_2 (0.5%) resulted in 34% Pb removal after 15 min which increased to 89% after 60 min. When the concentration of H_2O_2 increased to 5% and 10%, more than 90% removal was attained within a short period of 15 min. Instead, for RhB, the removal was negligible in the presence of Fe_3O_4@MgO without H_2O_2. However, the removal of RhB increased to 75%, 85%, and 100% with the increase in H_2O_2 concentrations to 0.5%, 1%, and 10%, respectively.

It is clear from the XPS analysis that in the absence of H_2O_2, the adsorbent layer exists as MgO. Consequently, there will not be any bubble formation and thus, the system remains immobile. This implies that the bubble formation and subsequent mixing effect have a prominent role in the removal of pollutants. Moreover, when the concentration of H_2O_2 increased, the material started moving through the solution to capture Pb^{2+} ions along with the generation of bubbles.

Effect of Fe_3O_4@MgO

The effect of Fe_3O_4@MgO concentration (0.2–1 g L^{-1}) was evaluated at a fixed H_2O_2 concentration of 5% (Fig. 7B). A clear difference in the removal efficiency was observed during the initial period. Removal efficiencies of 0%, 46%, 63%, 80%, and 81% were observed with 0, 0.2, 0.4, 0.8, and 1 g L^{-1} of Fe_3O_4@MgO, respectively. A similar removal pattern was observed for RhB. This difference could be correlated with the lack of adsorption sites at a low dose of the material. The adsorption sites increased with the increase in adsorbent concentration and reaction with H_2O_2.

317 ***Effect of pH***

318 pH is another important parameter in the remediation process, and therefore experiments
319 were conducted at different initial pHs such as 2, 5, 7.5, 9, and 11 with the optimized condition of
320 H_2O_2 concentration of 5% and Fe_3O_4@MgO dose of 0.8 g L^{-1}. As in the previous cases, a
321 noticeable effect was observed at the initial time of 15 min. The removal efficiencies were 62%,
322 63%, 85%, 84%, and 83% at pH 2, 5, 7.5, 9, and 11, respectively for Pb^{2+} ion removal (Fig. 7C).
323 However, for RhB, removal efficiencies of 53%, 63%, 62%, 68%, and 89% were observed after
324 45 min at these pHs.

325 Since the isoelectric point of MgO is 11, the difference in the adsorption could not be
326 discussed in relation to the material property (Wang et al., 2017). Therefore, the removal
327 efficiencies under varying pH could be due to the different speciation of Pb^{2+}. The Pb species
328 exist as Pb^{2+}, $Pb(OH)^{+}$, $Pb(OH)_2^{0}$, and $Pb(OH)_3^{-}$ at pH < 6, 8, > 9, and > 12, respectively (Sheng
329 et al., 2009; Mohan et al., 2017). When the pH is less than 6, the major species is Pb^{2+}, and the
330 competitive adsorption between H^{+} and Pb^{2+} on the surface of the material leads to a low
331 adsorption capacity. Likewise, when the pH increases the precipitation of hydroxides occurs to
332 enhance the removal efficiency. This is further supported by the lower solubility product of
333 $Pb(OH)_2$ (ksp = 1.43×10^{-20}) than that of $Mg(OH)_2$ (5.61×10^{-12}) (Ponomarev et al., 2019).
334 Moreover, the electrostatic repulsion of RhB from the MgO surface at acidic pH results in
335 reduced removal. Similarly, electrostatic attraction between the positively charged RhB and the
336 negatively charged Fe_3O_4@MgO should enhance their removal at high pH (Liu et al., 2020).

337

338

339 **Fig. 7.**

3.5. Evaluation of Fe_3O_4@MgO-H_2O_2 practical application

To attain our third objective, the performance of the Fe_3O_4@MgO-H_2O_2 particles under environmentally relevant conditions, some supplementary experiments such as reusability, removal of other heavy metals, and removal efficiency in real groundwater (from a rural area in South Korea) and river water (collected from Hyeongsan River, South Korea) spiked with Pb^{2+} were studied. The physicochemical characteristics of the ground and river water are listed in Supporting Information (Table S1).

The results of the reusability test are shown in Supporting Information (Fig. S6). It was found that more than 90% of the initial Pb was removed in the first cycle, and subsequently, the adsorption capacity was reduced. This is likely due to the leaching of Mg ions from the surface of MgO@Fe_3O_4. In addition, the capacity of MgO@Fe_3O_4 for other heavy metals such as Cd, Ni, Zn, Co, and Cu was also investigated and the results are shown in Fig. 8A. As shown by the results, all the selected heavy metals could be removed effectively by the MgO@Fe_3O_4-H_2O_2 system. The experiments with ground and river water spiked with Pb^{2+} showed that there was no significant difference in the removal efficiencies between them even when they contained different co-existing or interfering ions (Fig. 8B), showing good environmental adaptation capability of the system.

Fig. 8.

The Fe_3O_4@MgO nanocomposite-H_2O_2 system possessed several advantages over other similar systems (Fe_3O_4@MnO_2-H_2O_2) (Kang et al., 2019; Ye et al., 2021a), the MgO based nanocomposites (Mohan et al., 2017; Rahdar et al., 2019; Liu et al., 2020; Guo and Bulin, 2021).

In contrast to other MgO-based materials and other adsorbents, the present system allowed superior activity for the removal of heavy metals concomitant with dyes without any external shaking. Most importantly, in comparison with the other micro-mixing systems, the present study doesn't require surfactants. We anticipate that the findings presented in this study will offer a promising strategy for the on-site removal of a variety of pollutants from contaminated water. Furthermore, it is proposed that the Fe_3O_4@MgO nanocomposite could be used along with other oxidants such as persulfate and ozone to induce the oxidation of pollutants. The increase of pH with the addition of Fe_3O_4@MgO to the aqueous solution will be beneficial for ozone activation. In the same way, polymeric membranes could also be fabricated with Fe_3O_4@MgO for water purification and other environmental applications.

4. Conclusions

We have verified that the Fe_3O_4@MgO nanocomposite is very effective in the generation of bubbles in the presence of H_2O_2. As a result, the generation of oxygen bubbles in the presence of H_2O_2 promoted the agitation of the solution containing Fe_3O_4@MgO. The bubble generation and the following self-mixing mechanism enhanced the simultaneous removal of both Pb^{2+} and rhodamine B with exceptional stability. The effect of H_2O_2 concentration and initial pH revealed that the adsorption was induced at a low H_2O_2 concentration of 0.05% and is effective over a wide pH range (2.5 to 11). The data obtained from the XPS and ICP-OES analyses showed that the adsorption of Pb^{2+} occurred via the cation exchange mechanism. The unfeasibility of the homogeneous Fenton reaction in this system showed that adsorption by Fe_3O_4@MgO is the predominant mechanism for the removal of RhB. The nearly similar removal efficiencies in pure, river, and groundwater matrices and for different heavy metals is an important advantage. Thus,

Fe_3O_4@MgO could be proposed as an efficient adsorbent for the removal of a variety of water contaminants from their sources.

Conflicts of interest

There are no conflicts to declare

Acknowledgment

This research was supported by the National Research Foundation of Korea (NRF) grant funded by the Korean government (MEST) (No. 2017R1A2B3012681).

References

Abdullah, N., Yusof, N., Lau, W.J., Jaafar, J., Ismail, A.F., 2019. Recent trends of heavy metal removal from water/wastewater by membrane technologies. Journal of Industrial and Engineering Chemistry 76, 17-38.

Afroze, S., Sen, T.K., 2018. A Review on Heavy Metal Ions and Dye Adsorption from Water by Agricultural Solid Waste Adsorbents. Water, Air, & Soil Pollution 229, 225.

Alla, S.K., Verma, A.D., Kumar, V., Mandal, R.K., Sinha, I., Prasad, N.K., 2016. Solvothermal synthesis of CuO–MgO nanocomposite particles and their catalytic applications. RSC Advances 6, 61927-61933.

Calvo-Marzal, P., Sattayasamitsathit, S., Balasubramanian, S., Windmiller, J.R., Dao, C., Wang, J., 2010. Propulsion of nanowire diodes. Chemical Communications 46, 1623-1624.

Cao, C.-Y., Qu, J., Wei, F., Liu, H., Song, W.-G., 2012. Superb Adsorption Capacity and Mechanism of Flowerlike Magnesium Oxide Nanostructures for Lead and Cadmium Ions. ACS Applied Materials & Interfaces 4, 4283-4287.

Castro-Muñoz, R., González-Melgoza, L.L., García-Depraect, O., 2021. Ongoing progress on novel nanocomposite membranes for the separation of heavy metals from contaminated water. Chemosphere 270, 129421.

Chen, C., Karshalev, E., Guan, J., Wang, J., 2018. Magnesium-Based Micromotors: Water-Powered Propulsion, Multifunctionality, and Biomedical and Environmental Applications. Small 14, 1704252.

Chen, C.C., Chaudhary, A.J., Grimes, S.M., 2007. The effect of sodium hydroxide in photolytic and photocatalytic degradation of Acid Blue 29 and Ethyl Violet. Dyes and Pigments 73, 55-58.

Chen, X.-Z., Hoop, M., Mushtaq, F., Siringil, E., Hu, C., Nelson, B.J., Pané, S., 2017. Recent developments in magnetically driven micro- and nanorobots. Applied Materials Today 9, 37-48.

Chinthala, M., Balakrishnan, A., Venkataraman, P., Manaswini Gowtham, V., Polagani, R.K., 2021. Synthesis and applications of nano-MgO and composites for medicine, energy, and environmental remediation: a review. Environmental Chemistry Letters 19, 4415-4454.

Deng, H., Li, X., Peng, Q., Wang, X., Chen, J., Li, Y., 2005. Monodisperse Magnetic Single-Crystal Ferrite Microspheres. Angewandte Chemie International Edition 44, 2782-2785.

Dotto, J., Fagundes-Klen, M.R., Veit, M.T., Palácio, S.M., Bergamasco, R., 2019. Performance of different coagulants in the coagulation/flocculation process of textile wastewater. Journal of Cleaner Production 208, 656-665.

Gao, C., Zhang, W., Li, H., Lang, L., Xu, Z., 2008. Controllable Fabrication of Mesoporous MgO with Various Morphologies and Their Absorption Performance for Toxic Pollutants in Water. Crystal Growth & Design 8, 3785-3790.

Gao, W., Feng, X., Pei, A., Gu, Y., Li, J., Wang, J., 2013a. Seawater-driven magnesium based Janus micromotors for environmental remediation. Nanoscale 5, 4696-4700.

Gao, W., Sattayasamitsathit, S., Orozco, J., Wang, J., 2013b. Efficient bubble propulsion of polymer-based microengines in real-life environments. Nanoscale 5, 8909-8914.

Ghaedi, S., Seifpanahi-Shabani, K., Sillanpää, M., 2022. Waste-to-Resource: New application of modified mine silicate waste to remove Pb2+ ion and methylene blue dye, adsorption properties, mechanism of action and recycling. Chemosphere 292, 133412.

Grosvenor, A.P., Kobe, B.A., Biesinger, M.C., McIntyre, N.S., 2004. Investigation of multiplet splitting of Fe 2p XPS spectra and bonding in iron compounds. Surface and Interface Analysis 36, 1564-1574.

Guo, T., Bulin, C., 2021. Facile preparation of MgO/graphene oxide nanocomposite for efficient removal of aqueous Congo red: adsorption performance and interaction mechanism. Research on Chemical Intermediates 47, 945-971.

Iqbal, J., Shah, N.S., Sayed, M., Niazi, N.K., Imran, M., Khan, J.A., Khan, Z.U.H., Hussien, A.G.S., Polychronopoulou, K., Howari, F., 2021. Nano-zerovalent manganese/biochar composite for the adsorptive and oxidative removal of Congo-red dye from aqueous solutions. Journal of Hazardous Materials 403, 123854.

Joseph, L., Jun, B.-M., Flora, J.R.V., Park, C.M., Yoon, Y., 2019. Removal of heavy metals from water sources in the developing world using low-cost materials: A review. Chemosphere 229, 142-159.

Kameda, K., Hashimoto, Y., Ok, Y.S., 2018. Stabilization of arsenic and lead by magnesium oxide (MgO) in different seawater concentrations. Environmental Pollution 233, 952-959.

Kang, Y.-G., Yoon, H., Lee, C.-S., Kim, E.-J., Chang, Y.-S., 2019. Advanced oxidation and adsorptive bubble separation of dyes using MnO2-coated Fe3O4 nanocomposite. Water Research 151, 413-422.

Khairallah, F., Glisenti, A., Natile, M.M., Galenda, A., 2012. CuO/MgO Nanocomposites by Wet Impregnation: An XPS Study. Surface Science Spectra 19, 23-29.

Kim, E.-J., Lee, C.-S., Chang, Y.-Y., Chang, Y.-S., 2013. Hierarchically Structured Manganese Oxide-Coated Magnetic Nanocomposites for the Efficient Removal of Heavy Metal Ions from Aqueous Systems. ACS Applied Materials & Interfaces 5, 9628-9634.

Kim, S., Park, C.M., Jang, M., Son, A., Her, N., Yu, M., Snyder, S., Kim, D.-H., Yoon, Y., 2018. Aqueous removal of inorganic and organic contaminants by graphene-based nanoadsorbents: A review. Chemosphere 212, 1104-1124.

Lai, H., Deng, J., Wen, S., Liu, Q., 2019. Elucidation of lead ions adsorption mechanism on marmatite surface by PCA-assisted ToF-SIMS, XPS and zeta potential. Minerals Engineering 144, 106035.

Lee, C.-S., Gong, J., Oh, D.-S., Jeon, J.-R., Chang, Y.-S., 2018. Zerovalent-Iron/Platinum Janus Micromotors with Spatially Separated Functionalities for Efficient Water Decontamination. ACS Applied Nano Materials 1, 768-776.

Li, J., Singh, V.V., Sattayasamitsathit, S., Orozco, J., Kaufmann, K., Dong, R., Gao, W., Jurado-Sanchez, B., Fedorak, Y., Wang, J., 2014. Water-Driven Micromotors for Rapid Photocatalytic Degradation of Biological and Chemical Warfare Agents. ACS Nano 8, 11118-11125.

Lin, J.X., Wang, L., 2009. Adsorption of dyes using magnesium hydroxide-modified diatomite. Desalination and Water Treatment 8, 263-271.

Liu, M., Zentgraf, T., Liu, Y., Bartal, G., Zhang, X., 2010. Light-driven nanoscale plasmonic motors. Nature Nanotechnology 5, 570-573.

Liu, N., Wu, Y., Sha, H., 2020. Magnesium oxide modified diatomite waste as an efficient adsorbent for organic dye removal: adsorption performance and mechanism studies. Separation Science and Technology 55, 234-246.

Malik, V., Saya, L., Gautam, D., Sachdeva, S., Dheer, N., Arya, D.K., Gambhir, G., Hooda, S., 2022. Review on adsorptive removal of metal ions and dyes from wastewater using tamarind-based bio-composites. Polymer Bulletin.

Mohan, S., Kumar, V., Singh, D.K., Hasan, S.H., 2017. Effective removal of lead ions using graphene oxide-MgO nanohybrid from aqueous solution: Isotherm, kinetic and thermodynamic modeling of adsorption. Journal of Environmental Chemical Engineering 5, 2259-2273.

Mou, F., Chen, C., Ma, H., Yin, Y., Wu, Q., Guan, J., 2013. Self-Propelled Micromotors Driven by the Magnesium–Water Reaction and Their Hemolytic Properties. Angewandte Chemie International Edition 52, 7208-7212.

Nadeem, M., Mahmood, A., Shahid, S.A., Shah, S.S., Khalid, A.M., McKay, G., 2006. Sorption of lead from aqueous solution by chemically modified carbon adsorbents. Journal of Hazardous Materials 138, 604-613.

Nigam, P., Banat, I.M., Singh, D., Marchant, R., 1996. Microbial process for the decolorization of textile effluent containing azo, diazo and reactive dyes. Process Biochemistry 31, 435-442.

Osagie, C., Othmani, A., Ghosh, S., Malloum, A., Kashitarash Esfahani, Z., Ahmadi, S., 2021. Dyes adsorption from aqueous media through the nanotechnology: A review. Journal of Materials Research and Technology 14, 2195-2218.

Peng, H., Wang, X., Hu, C., Hu, J., Tian, X., 2016. A simple approach for the synthesis of bi-functional Fe3O4@MgO core–shell nanoparticles with magnetic-microwave to heat responsive properties. New Journal of Chemistry 40, 7911-7916.

Ponomarev, N., Pastushok, O., Repo, E., Doshi, B., Sillanpää, M., 2019. Lignin-Based Magnesium Hydroxide Nanocomposite. Synthesis and Application for the Removal of Potentially Toxic Metals from Aqueous Solution. ACS Applied Nano Materials 2, 5492-5503.

Qiu, B., Tao, X., Wang, H., Li, W., Ding, X., Chu, H., 2021. Biochar as a low-cost adsorbent for aqueous heavy metal removal: A review. Journal of Analytical and Applied Pyrolysis 155, 105081.

Rahdar, S., Rahdar, A., Zafar, M.N., Shafqat, S.S., Ahmadi, S., 2019. Synthesis and characterization of MgO supported Fe–Co–Mn nanoparticles with exceptionally high adsorption capacity for Rhodamine B dye. Journal of Materials Research and Technology 8, 3800-3810.

Rasaki, S.A., Bingxue, Z., Guarecuco, R., Thomas, T., Minghui, Y., 2019. Geopolymer for use in heavy metals adsorption, and advanced oxidative processes: A critical review. Journal of Cleaner Production 213, 42-58.

Safdar, M., Wani, O.M., Jänis, J., 2015. Manganese Oxide-Based Chemically Powered Micromotors. ACS Applied Materials & Interfaces 7, 25580-25585.

Sánchez, S., Soler, L., Katuri, J., 2015. Chemically Powered Micro- and Nanomotors. Angewandte Chemie International Edition 54, 1414-1444.

Sasaki, K., Fukumoto, N., Moriyama, S., Hirajima, T., 2011. Sorption characteristics of fluoride on to magnesium oxide-rich phases calcined at different temperatures. Journal of Hazardous Materials 191, 240-248.

Sasi, S., Rayaroth, M.P., Aravindakumar, C.T., Aravind, U.K., 2021. Alcohol ethoxysulfates (AES) in environmental matrices. Environmental Science and Pollution Research 28, 34167-34186.

Sheng, G., Wang, S., Hu, J., Lu, Y., Li, J., Dong, Y., Wang, X., 2009. Adsorption of Pb(II) on diatomite as affected via aqueous solution chemistry and temperature. Colloids and Surfaces A: Physicochemical and Engineering Aspects 339, 159-166.

Vakili, M., Rafatullah, M., Ibrahim, M.H., Abdullah, A.Z., Salamatinia, B., Gholami, Z., 2014. Oil Palm Biomass as an Adsorbent for Heavy Metals. in: Whitacre, D.M. (Ed.). Reviews of Environmental Contamination and Toxicology Volume 232. Springer International Publishing, Cham, pp. 61-88.

Valix, M., Cheung, W.H., McKay, G., 2004. Preparation of activated carbon using low temperature carbonisation and physical activation of high ash raw bagasse for acid dye adsorption. Chemosphere 56, 493-501.

Vilela, D., Parmar, J., Zeng, Y., Zhao, Y., Sánchez, S., 2016. Graphene-Based Microbots for Toxic Heavy Metal Removal and Recovery from Water. Nano Letters 16, 2860-2866.

Vilela, D., Stanton, M.M., Parmar, J., Sánchez, S., 2017. Microbots Decorated with Silver Nanoparticles Kill Bacteria in Aqueous Media. ACS Applied Materials & Interfaces 9, 22093-22100.

Wang, B., Xiong, X., Ren, H., Huang, Z., 2017. Preparation of MgO nanocrystals and catalytic mechanism on phenol ozonation. RSC Advances 7, 43464-43473.

Wang, H., Pumera, M., 2015. Fabrication of Micro/Nanoscale Motors. Chemical Reviews 115, 8704-8735.

Xu, T., Xu, L.-P., Zhang, X., 2017. Ultrasound propulsion of micro-/nanomotors. Applied Materials Today 9, 493-503.

Ye, H., Kang, J., Ma, G., Sun, H., Wang, S., 2018. High-speed graphene@Ag-MnO2 micromotors at low peroxide levels. Journal of Colloid and Interface Science 528, 271-280.

543 Ye, H., Sun, H., Wang, S., 2017. Electrochemical synthesis of graphene/MnO2 in an architecture
544 of bilayer microtubes as micromotors. Chemical Engineering Journal 324, 251-258.
545 Ye, H., Wang, Y., Liu, X., Xu, D., Yuan, H., Sun, H., Wang, S., Ma, X., 2021a. Magnetically
546 steerable iron oxides-manganese dioxide core–shell micromotors for organic and microplastic
547 removals. Journal of Colloid and Interface Science 588, 510-521.
548 Ye, S., Chen, Y., Yao, X., Zhang, J., 2021b. Simultaneous removal of organic pollutants and
549 heavy metals in wastewater by photoelectrocatalysis: A review. Chemosphere 273, 128503.
550 Yu, X.-Y., Luo, T., Jia, Y., Zhang, Y.-X., Liu, J.-H., Huang, X.-J., 2011. Porous Hierarchically
551 Micro-/Nanostructured MgO: Morphology Control and Their Excellent Performance in As(III)
552 and As(V) Removal. The Journal of Physical Chemistry C 115, 22242-22250.
553 Zazou, H., Afanga, H., Akhouairi, S., Ouchtak, H., Addi, A.A., Akbour, R.A., Assabbane, A.,
554 Douch, J., Elmchaouri, A., Duplay, J., Jada, A., Hamdani, M., 2019. Treatment of textile industry
555 wastewater by electrocoagulation coupled with electrochemical advanced oxidation process.
556 Journal of Water Process Engineering 28, 214-221.
557 Zeng, W., Yin, Z., Gao, M., Wang, X., Feng, J., Ren, Y., Wei, T., Fan, Z., 2020. In-situ growth of
558 magnesium peroxide on the edge of magnesium oxide nanosheets: Ultrahigh photocatalytic
559 efficiency based on synergistic catalysis. Journal of Colloid and Interface Science 561, 257-264.

560
561

562 **Figure captions**

563

564 **Fig. 1.** Scanning electron microscopy images (A and B), energy dispersive X-ray spectra (C), and
565 X-ray diffraction pattern (D) of Fe_3O_4@MgO nanocomposites.

566

567 **Fig. 2.** Mg 1s X-ray photoelectron spectroscopy (XPS) spectra (A and C) and O 1s XPS spectra
568 (B and D) of Fe_3O_4@MgO before and after H_2O_2 treatment.

569

570 **Fig. 3.** Photographic images of bubble formation with the addition of Fe_3O_4@MgO in the
571 solution containing H_2O_2; 1 s (A), 60 s (B), and 90 s (C). Microscopic images (scale bar 10 μm)
572 of bubble generation with the addition of 0.05% (D), 0.5% (E), 1% (F), 2% (G), 5% (H), and
573 10% (I) H_2O_2.

574

575 **Fig. 4.** Time-dependent changes in the pH (A) and dissolved oxygen (DO) (B) of deionized water
576 in the Fe_3O_4@MgO-H_2O_2 system. Experimental conditions: [Fe_3O_4@MgO] = 0.8 g/L, [H_2O_2] =
577 5%.

578

579 **Fig. 5.** Simultaneous removal of Pb^{2+} and RhB by Fe_3O_4@MgO with the addition of H_2O_2.
580 Experimental conditions: [Fe_3O_4@MgO] = 0.8 g L^{-1}, [H_2O_2] = 5%, and [Pollutants] = 10 mg L^{-1}.

581

582 **Fig. 6.** Time-dependent release of Mg^{2+} ions from Fe_3O_4@MgO during the adsorption reaction
583 (A) and X-ray photoelectron spectroscopy of Pb 4f spectra of Fe_3O_4@MgO particles after the

adsorption of Pb^{2+} (B). Experimental conditions: [Fe_3O_4@MgO] = 0.8 g L^{-1}, [H_2O_2] = 5%, and [Pb^{2+}] = 10 mg $L^{-1.}$

Fig. 7. Effect of H_2O_2 (A), TX-100 (B), Fe_3O_4@MgO dose (C), and pH (D) on the removal of Pb^{2+} in the Fe_3O_4@MgO-H_2O_2 system. Experimental conditions: [Pb^{2+}] = 10 mg $L^{-1.}$

Fig. 8. Removal of Pb^{2+} from deionized, ground, and river water (A) and removal efficiency of various heavy metals (B) by the Fe_3O_4@MgO–H_2O_2 system. Experimental conditions: [Fe_3O_4@MgO] = 0.8 g L^{-1}, [H_2O_2] = 5%, [Pb^{2+}] = 10 mg L^{-1}, and pH 7.5

Figures

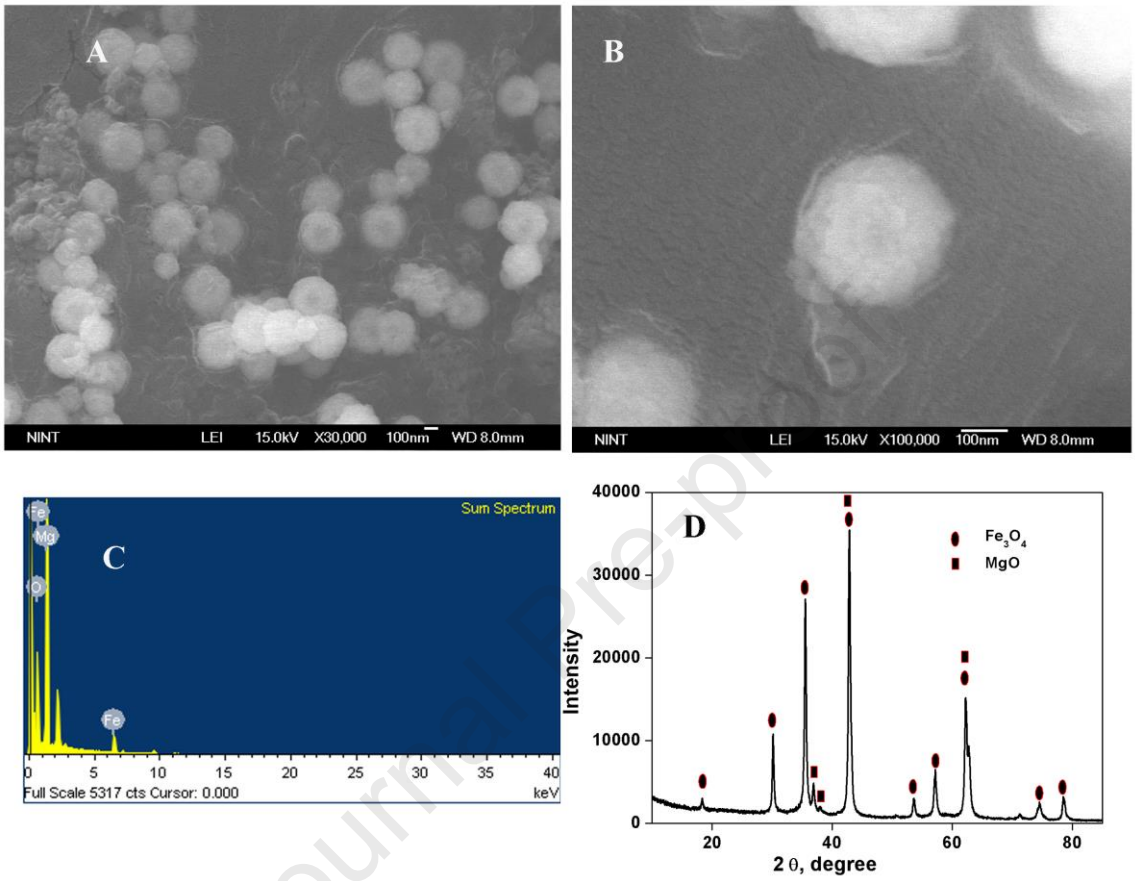

Fig. 1

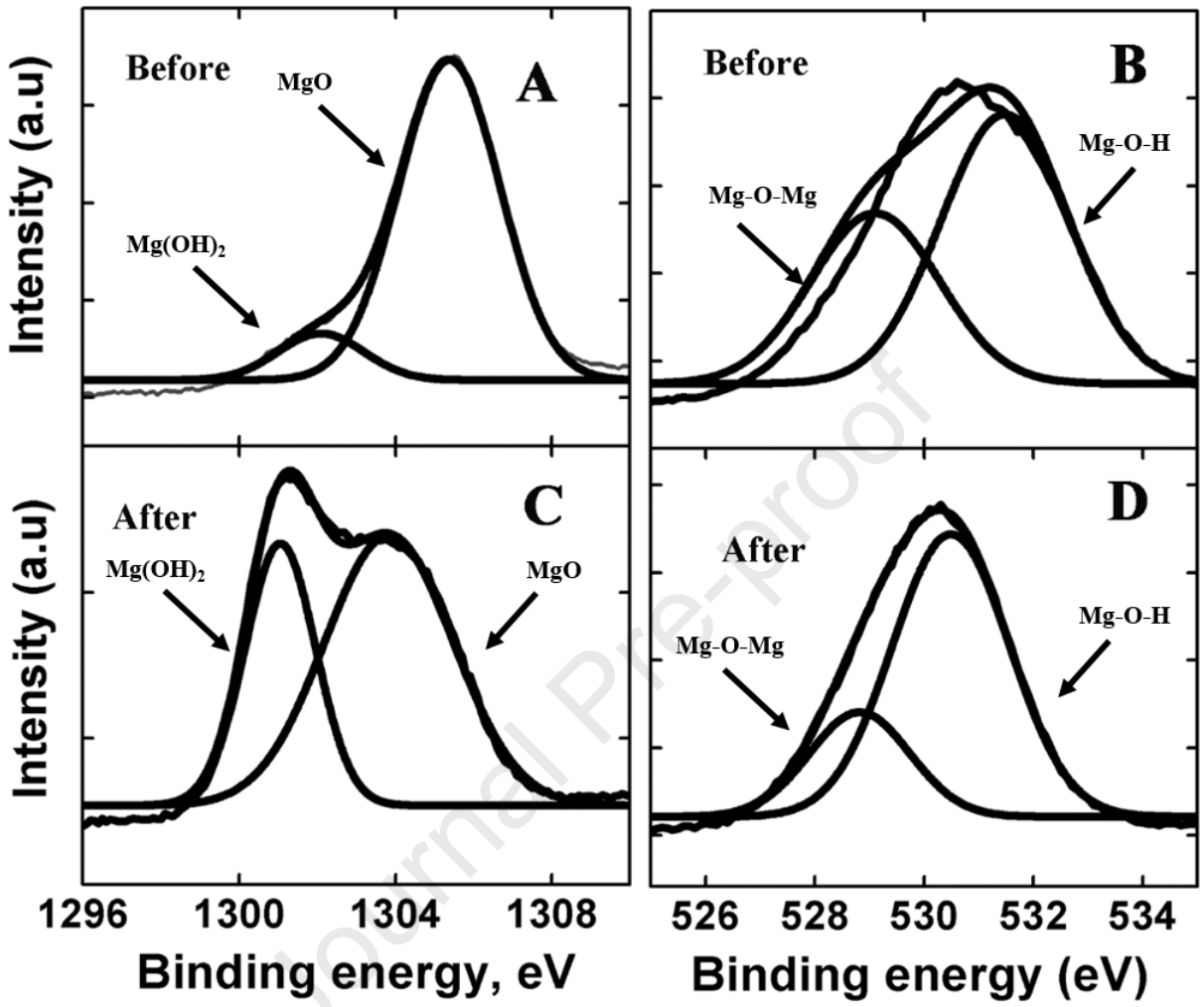

Fig. 2

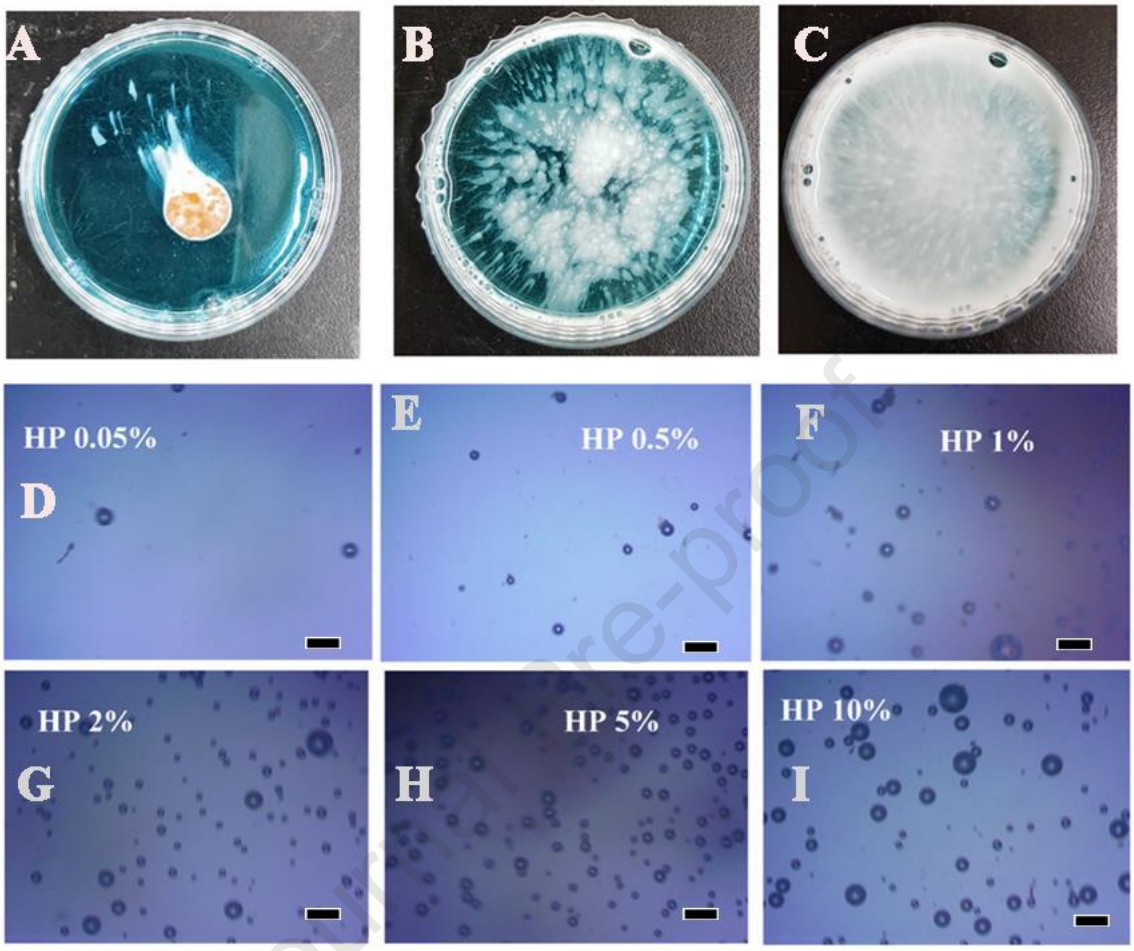

Fig. 3

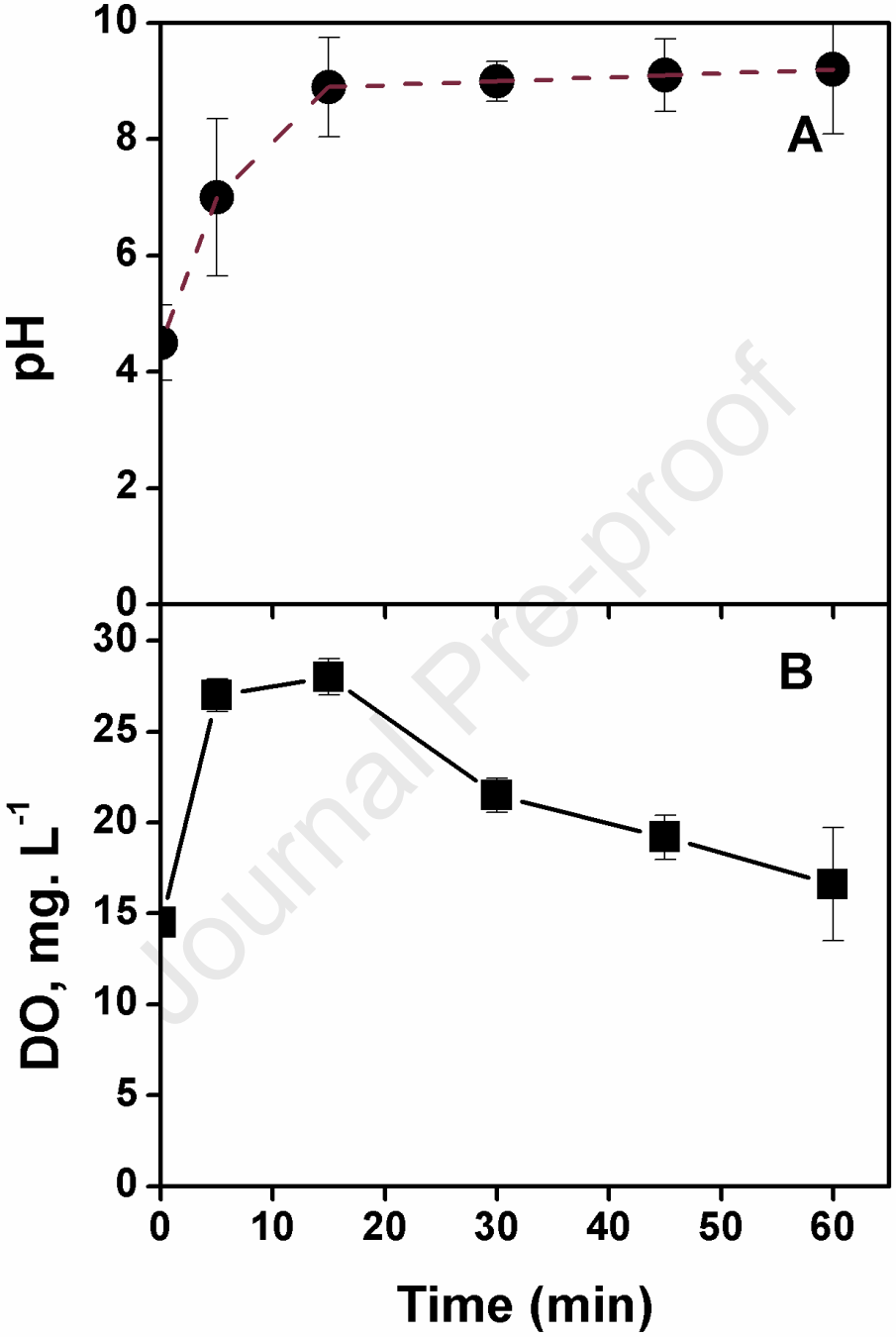

Fig. 4

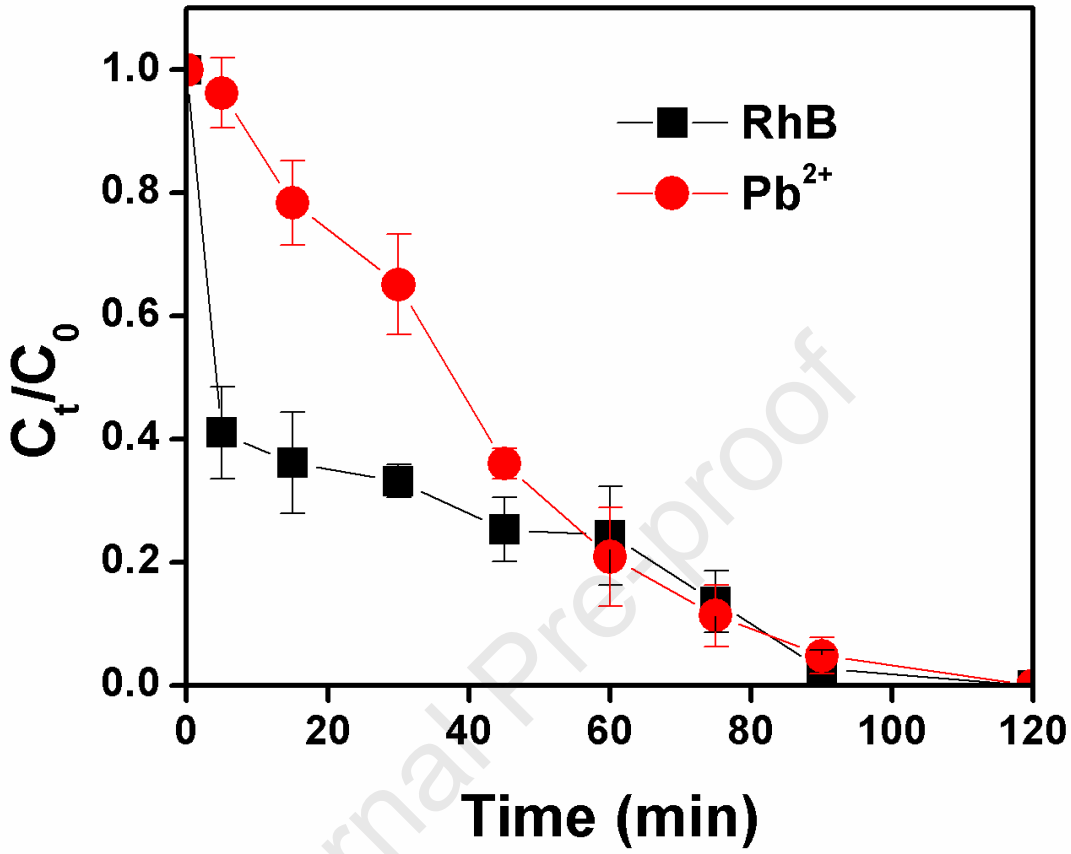

Fig. 5

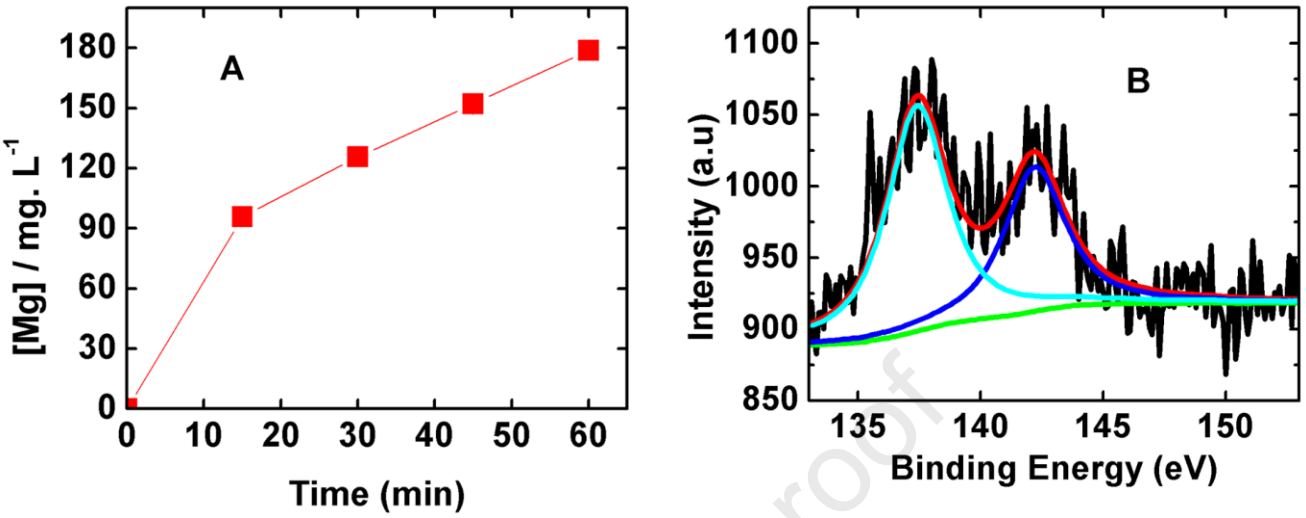

Fig. 6

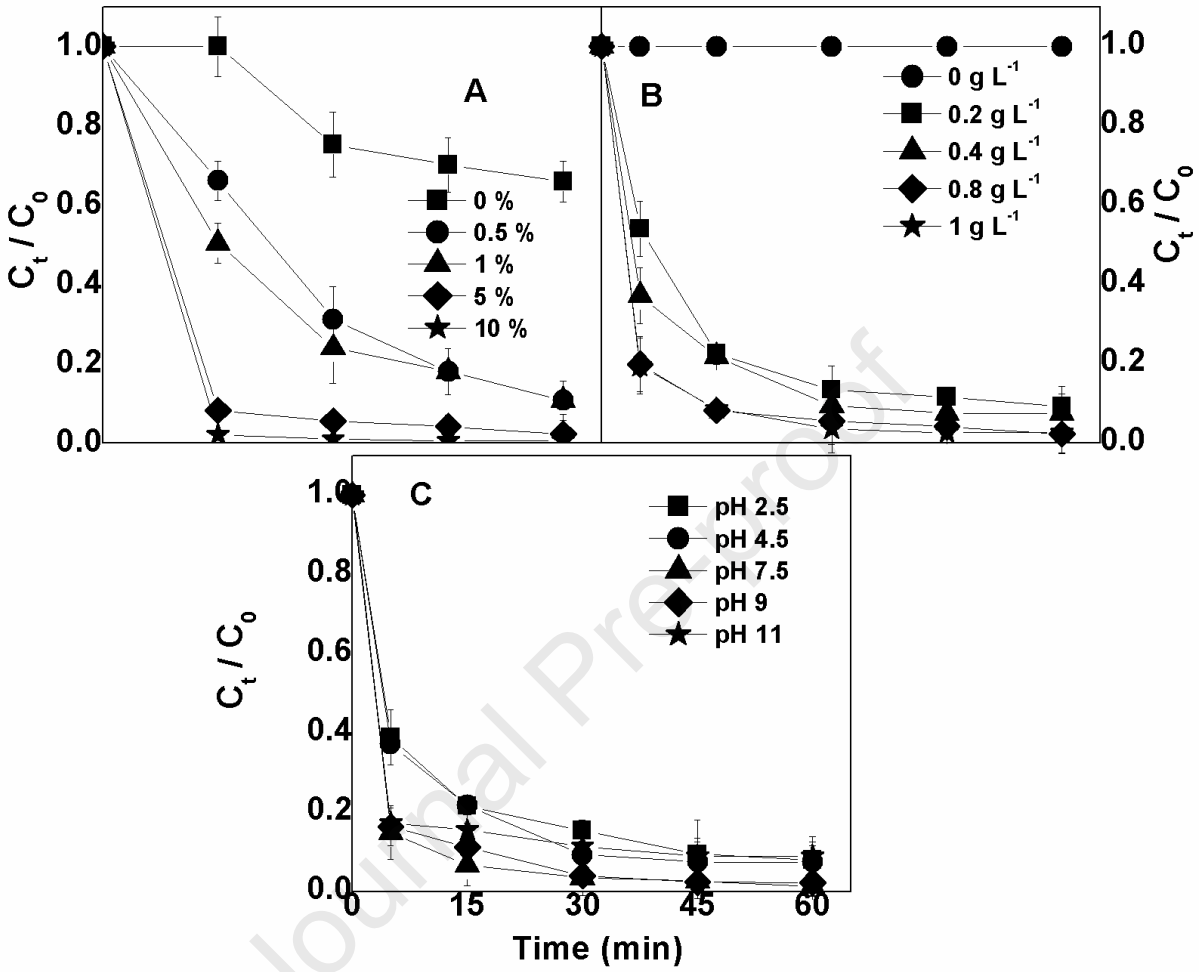

Fig. 7

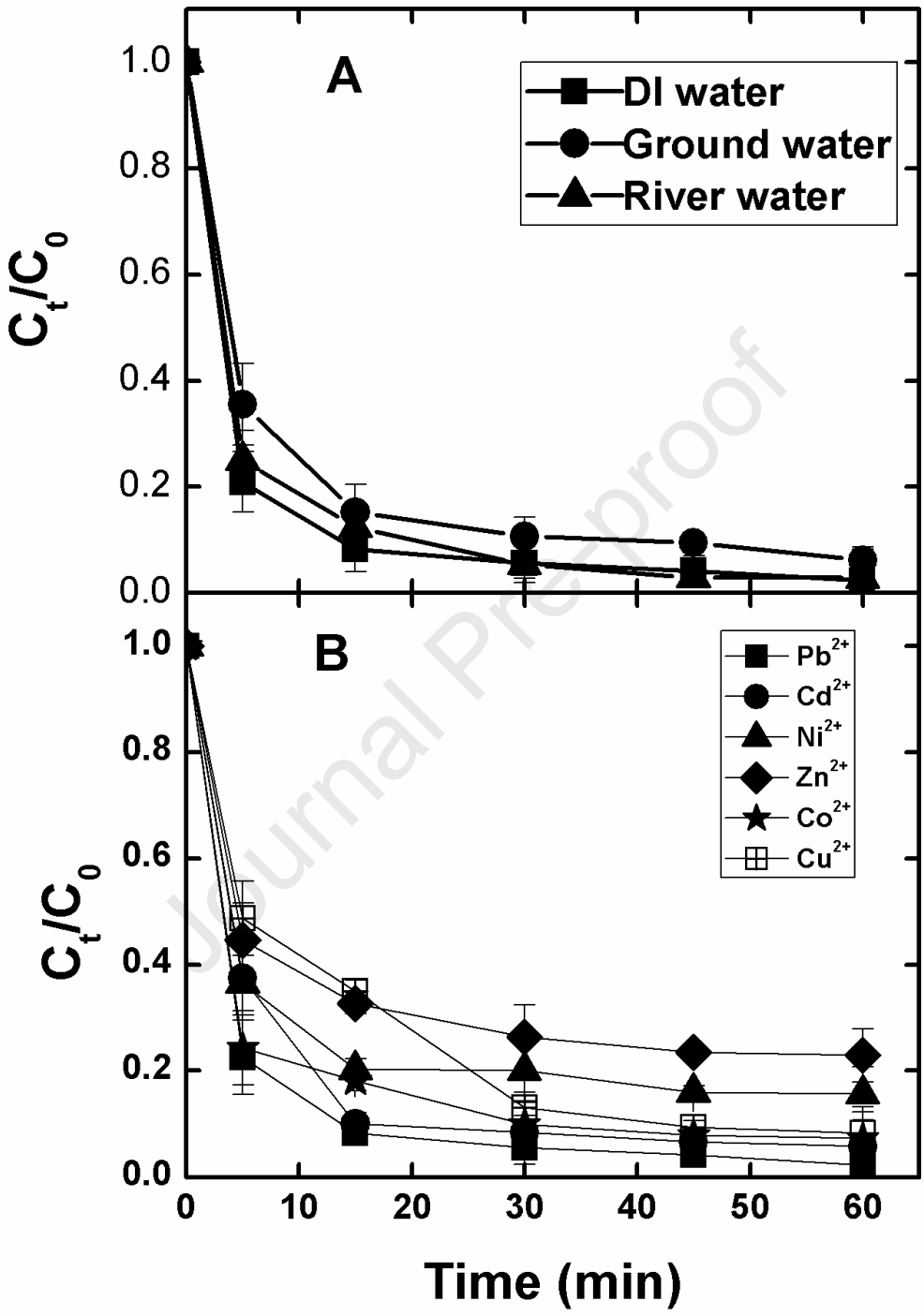

Fig. 8

Highlights

- Heavy metal (Pb^{2+}) and organic dye (Rhodamine B) removal with H_2O_2 addition to the solution containing Fe_3O_4@MgO.
- Pollutants are removed by the adsorption mechanism.
- The bubble propulsion and self-mixing process enhanced the removal efficiency.
- Fe_3O_4@MgO is efficient in environmentally relevant water matrices like ground and river water.